Rapid evolution of an overt metabolic defect restores balanced growth

Robin Green [1*], Wenyun Lu [2#], Lin Wang [2#], Samuel F.M. Hart [1#]
David Skelding [1], Justin C. Burton [1], Aric Capel [1], Hung Alex Chen [1], Aaron Lin [1]
Arvind R. Subramaniam [1], Joshua D. Rabinowitz [2], Wenying Shou [1*]
[1]: Division of Basic Sciences, Fred Hutch Cancer Research Center, Seattle, WA, USA
[2]: Department of Chemistry and Lewis-Sigler Institute for Integrative Genomics, Princeton University, Princeton, NJ, USA
[*]: Author of correspondence; [#]: Equal contribution

Abstract

In eukaryotes, conserved mechanisms ensure that cell growth is coordinated with nutrient availability. Overactive growth during nutrient limitation leads to rapid cell death. Here, we demonstrate that cells can adapt to this nutrient-growth imbalance by evolving major metabolic defects. Specifically, when yeast lysine auxotrophic mutant *lys*$^-$ suffered nutrient-growth imbalance in limited lysine, a sub-population repeatedly evolved to lose the ability to synthesize organosulfurs (*lys*$^-$*orgS*$^-$). Organosulfurs, mainly glutathione and glutathione conjugates, were released by *lys*$^-$ cells during lysine limitation when nutrient-growth is imbalanced, but not during glucose limitation when nutrient-growth is balanced. Limiting organosulfurs conferred a frequency-dependent fitness advantage to *lys*$^-$*orgS*$^-$ by eliciting a proper slow growth program including autophagy. Thus, nutrient-growth imbalance can trigger rapid niche construction, which in turn enables the selection of an overt metabolic defect to better tune cell growth to the metabolic environment.

Introduction

All organisms must sense the availability of nutrients. In eukaryotes, when nutrients are abundant, cells express growth-promoting genes associated with, for example, protein synthesis and mitochondrial function, and grow [1]. When nutrients are limited, cells launch stress-response programs and undergo, for example, quiescence and autophagy [1,2]. Mechanisms that ensure this coordination between nutrient availability and growth, or nutrient-growth balance, are conserved across eukaryotes [3].

Slowing growth during nutrient limitation is essential for cell survival. If cells attempt to grow despite being limited for essential metabolites, they could suffer rapid death from this nutrient-growth imbalance. For example in *S. cerevisiae*, when a nutrient required by all cells (e.g. carbon[4], nitrogen[5], or sulfur [6]) is limiting ("natural limitation"), cells slow down growth and thus survive. In contrast, when an auxotrophic mutant is limited for the essential metabolite that it has lost the ability to make ("unnatural limitation"), often the mutant fails to slow down growth and consequently suffers significantly reduced viability compared to viability during natural limitation [7,8]. Nutrient-growth imbalance is in part due to erroneous activation of the growth activator TORC1 (Target of Rapamycin Complex 1) during unnatural limitation. Inactivating TORC1, which can be achieved by loss-of-function mutations in the TORC1 pathway or by applying the TORC1 inhibitor rapamycin, restores cell viability [7].

Since nutrient-growth balance is regulated in a conserved fashion across eukaryotes, and since some cancers are believed to suffer nutrient-growth imbalance[9], we investigate how cells suffering nutrient-

growth imbalance might evolve, taking advantage of a yeast auxotroph mutant.

Results

Nutrient-growth imbalance in *lys-* cells during lysine limitation

To examine how cells might cope with nutrient-growth imbalance, we took advantage of a lysine auxotrophic yeast strain where the *LYS2* gene has been deleted ("*lys*$^-$"). Consistent with previous work [8], *lys*$^-$ cells starved for lysine died rapidly (Fig 1A, dark blue circles), although *lys*$^-$ cells simultaneously starved for lysine and carbon died slowly (Fig 1A, green circles). This is presumably because carbon shortage allowed cells to enter the proper state of no growth (Fig 1A, ii), while lysine starvation – an unnatural limitation – was not properly sensed, and consequently cells would attempt to grow despite lysine shortage and die (Fig 1A, iii). Expression of genes associated with autophagy, a process where the degradation and recycling of cellular components facilitates stress survival, was reduced during nutrient-growth imbalance, which could also contribute to low cell viability [8]. Indeed, poor cell viability was rescued by rapamycin which inhibited TORC1, a growth promoter and autophagy inhibitor (Fig 1A, blue crosses; i). In summary, *lys*$^-$ cells limited for lysine suffered nutrient-growth imbalance and poor viability.

Evolution of organosulfur auxotrophy in nutrient-growth dysregulated cells

To examine how cells might cope with nutrient-growth imbalance, we evolved *lys*$^-$ cells in lysine-limited chemostats for tens of generations (Methods, "Evolution"; "Chemostats and turbidostats"). We then randomly chose a total of ~70 evolved clones for whole-genome sequencing. Similar to our previous findings [10], each clone carried at least one mutation that increased the cell's affinity for lysine. These mutations included gaining an extra copy of chromosome 14 which harbors the high-affinity lysine permease gene *LYP1* [12], or losing or reducing activities of genes involved in degrading Lyp1 (e.g. *ECM21*, *RSP5*, and *DOA4*) [11] (Table S2).

Surprisingly, even though the medium originally contained no organosulfurs (sulfur-containing organic molecules; Fig S1), ~10% of the ~70 sequenced clones also harbored mutations in the biosynthetic pathway that converts externally-supplied sulfate to organosulfurs essential to cell viability. These mutations included *met10*, *met14*, and *met17* (Fig 1B). Indeed, these mutant clones required an external source of organosulfur such as methionine to grow (Fig 1B), consistent with previous findings [13]. We designate these mutants as *lys*$^-$*orgS*$^-$. Since our growth medium was not supplemented with any organosulfurs, *lys*$^-$*orgS*$^-$ cells must have received organosulfur(s) from *lys*$^-$ cells in the same culture which are capable of synthesizing organosulfurs. Since *lys*$^-$ and *lys*$^-$*orgS*$^-$ clones from the same culture harbored identical *ecm21 or rsp5* mutation (Table S2, matched color shading), *ecm21* or *rsp5* mutation arose first, followed by *orgS*$^-$. When we tested three independent chemostat cultures and three independent cross-feeding communities at 30~80 generations, *lys*$^-$*orgS*$^-$ mutants could be detected in all cases (Fig S2; Methods "Quantifying auxotroph frequency").

The organosulfur niche mainly consists of glutathione S-conjugates and glutathione

We sought to identify the released organosulfurs ("organosulfur niche") in chemostat supernatants. When ancestral *lys*$^-$ cells were cultured in lysine-limited chemostats, organosulfurs rapidly accumulated in the supernatant and reached a steady-state (Fig S3). Using liquid chromatography-mass spectrometry (Methods, "LC-MS"), we identified glutathione as a released organosulfur (Fig 2A). Glutathione (GSH) is a tri-peptide comprising glutamate, cysteine (containing –SH), and glycine. In the cell, GSH is a major redox buffer, and can form sulfur-conjugates with itself (GS-SG) and with other compounds via disulfide bonds (e.g. GS-S-CoA) [14]. Consistent with LC-MS results, *gsh1*- cells, whose growth can be supported by externally-supplied GSH or GSH S-conjugates (GS-X) but not methionine (Fig S1, Fig S4) [15], grew in chemostat supernatants (Fig S4E).

Further chemical analysis revealed that the organosulfur niche contained mainly GS-X and some GSH. Specifically, we estimated the total organosulfur niche using a yield-based bioassay (Methods, "Bioassays"). We used *met10*$^-$, a mutant isolated in our evolution experiment which can use GSH, GS-X, and non-GSH organosulfurs such as methionine (Fig S4). By comparing the final turbidity of *met10*$^-$ in a chemostat supernatant versus in various known amounts of GSH, we can estimate the organosulfur niche in terms of GSH equivalents (Fig 2B, i). We then quantified GSH using HPLC and LC-MS (Fig 2B, ii and iii; Methods, "HPLC", "LC-MS"). Finally, we quantified the total abundance of GSH and GS-X by chemically reducing GS-X to GSH (Methods) and then measuring total GSH via LC-MS (Fig 2B, iv). GSH and GS-X together dominated the organosulfur niche (Fig 2B, compare i and iv), with GS-X being the major component (Fig 2B, compare iii with iv).

The organosulfur niche was mainly created by live cell release rather than by cell lysis. Specifically, we compared the organosulfur concentration quantified in supernatant (Fig 2C, brown) with that attributable to dead cell release (Fig 2C, purple; calculated by multiplying intracellular organosulfur content with dead cell density). Our measurements suggest that organosulfurs were mainly released by live cells (Fig 2C; Fig S6), consistent with the observation that GSH and GS-X are exported from the cell in an ATP-dependent fashion [14,16].

Organosulfur release is associated with nutrient-growth imbalance

To test whether organosulfur release is associated with nutrient-growth imbalance or with slow growth, we grew *lys*$^-$ cells in glucose-limited chemostats and lysine-limited chemostats at the same doubling time. In contrast to lysine limitation, in glucose limitation nutrient-growth balance is normal and percent dead cells is lower (Fig 1A; Fig 3A). Organosulfurs accumulated to steady state in lysine-limited chemostats but were undetectable in glucose-limited chemostats, despite the latter's higher steady-state live population density (Fig 3). As a further test, we grew *lys*- cells in nutrient-rich turbidostats [17] (Methods, "Chemostats and turbidostats") where cells grow fast in excess nutrients and thus nutrient-growth balance is achieved. *lys2*- cells in nutrient-rich turbidostats released GSH at a much slower rate than in lysine-limited chemostats (Fig S5). Taken together, these results suggest that organosulfur release is associated with nutrient-growth imbalance.

Organosulfur limitation confers a frequency-dependent fitness advantage to *orgS*$^-$

How might *lys*$^-$*orgS*$^-$ rise from the original mutant cell to a detectable frequency during lysine limitation? To directly test whether *orgS*$^-$ mutation conferred fitness benefit to *lys*- cells, we restored *met10* to

MET10 in an evolved *lys*$^-$*orgS*$^-$ clone, and compared isogenic *lys*$^-$*orgS*$^-$ and *lys*$^-$ clones in a variety of nutrient environments. According to the prevalent "energy saving" hypothesis [18,19], *lys*$^-$*orgS*$^-$ might be spared of the cost of *de novo* synthesis of organosulfurs by utilizing external organosulfurs. If this was true, then excess organosulfurs should help *lys*$^-$*orgS*$^-$ to perhaps be even more fit than *lys*$^-$. However, we observed the opposite: when both lysine and GSH were in excess, *lys*$^-$*orgS*$^-$ grew significantly slower than *lys*$^-$ (Fig 4A). During lysine limitation, *lys*$^-$*orgS*$^-$ survived better than *lys*$^-$ during organosulfur limitation (Fig 4B orange open circles higher than blue open circles), but *lys*$^-$*orgS*$^-$ survived poorly when organosulfur was in excess (Fig 4B compare open and filled orange circles; Fig S8). A similar trend was observed at intermediate levels of lysine and GSH (Fig S9).

An alternative hypothesis is that organosulfur limitation restored nutrient-growth balance in *lys*$^-$*orgS*$^-$ during lysine limitation, thus conferring *lys*$^-$*orgS*$^-$ a fitness advantage over the nutrient-growth imbalanced *lys*$^-$. That is, organosulfur limitation posed a "natural limitation" which properly shut down growth as well as turned on stress-response pathways such as autophagy in *lys*$^-$*orgS*$^-$ cells. Consistent with this notion, the poor survival of *lys*$^-$*orgS*$^-$ in high organosulfur was rescued by growth inhibitor rapamycin (Fig 4B orange cross; Fig S8). Deletion of *ATG5*, a gene essential for autophagy, led to poor survival of *lys*$^-$*orgS*$^-$ cells despite growth inhibition by rapamycin (Fig 4B green; Fig S8).

To directly test any fitness difference between isogenic *lys*$^-$ and *lys*$^-$*orgS*$^-$ clones, we marked them with different fluorescent proteins, and competed them in lysine limitation (Methods. "Competition"). When *lys*$^-$*orgS*$^-$ was initially abundant, its frequency declined as expected (Fig 4C purple) due to competition for the limited organosulfurs released from rare *lys*$^-$. When *lys*$^-$*orgS*$^-$ was rare, its frequency initially increased (Fig 4 C red and green), demonstrating a fitness advantage over *lys*$^-$. Regardless of the initial value, the strain ratio converged to the steady state (Fig 4). The observed steady state ratio is consistent with organosulfur release and consumption measurements (Methods,"Competition"). Taken together, by restoring nutrient-growth balance, organosulfur limitation confers *lys*$^-$*orgS*$^-$ a negative frequency-dependent fitness advantage over *lys*$^-$ during lysine limitation.

Discussions

Our work demonstrates that a cell population with nutrient-growth imbalance (*lys*$^-$ cells in lysine limitation; Fig 1A) often diverged into two subpopulations within tens of generations: *lys*$^-$ and *lys*$^-$*orgS*$^-$ (Fig 1B and Fig S2). The probable sequence of events is the following: Upon lysine limitation, cells initially adapted to lysine limitation via mutations such as *ecm21*, *rsp5*, and *Disomy14* that increased the membrane abundance of the lysine permease Lyp1, and such mutations would become fixed in the culture. Live *lys*$^-$ cells released organosulfurs consisting primarily of GS-X and, to a less extent, GSH (Figs 2, S3, S5, and S6). This created an organosulfur niche. When *lys*$^-$*orgS*$^-$ (e.g. *lys*$^-$*met10*$^-$) arose by mutation, it could grow in the organosulfur niche (Fig S4). Initially, *lys*$^-$*orgS*$^-$ had a fitness advantage over *lys*$^-$ (Fig 4 and Fig). This is presumably because for *lys*$^-$*orgS*$^-$ cells, low concentrations of organosulfur mimicked natural sulfur limitation and thus slowed the over-active growth. Indeed, *lys*$^-$*orgS*$^-$ survived lysine

limitation better than *lys*$^-$ (Figs 4 and S8), and the superior survival of *lys*$^-$*orgS*$^-$ required autophagy (Figs 5 and S8). As *lys*$^-$*orgS*$^-$ increased to a higher frequency, its fitness advantage over *lys*$^-$ would diminish due to the increasing ratio of organosulfur consumer to organosulfur supplier. Eventually, a steady-state ratio of *lys*$^-$*orgS*$^-$:*lys*$^-$ could be reached (Fig 4), until new mutations alter the relative fitness between the two populations (Fig S2).

Chemical release by cells ("niche construction") mediates diverse microbial interactions [20–23]. Indeed, auxotrophs are predicted to be widespread [19,24] and have been found in natural isolates [25–30]. Often, metabolites are released as a consequence of "overflow" metabolism [31–35]. For example, yeast excretes amino acids as a consequence of nitrogen overflow, and the released amino acids in turn enable the survival of symbiotic lactic acid bacteria [32]. The release of GSH and GS-X by lysine-limited *lys*$^-$ cells is likely a consequence of nutrient-growth imbalance (Fig 3, Fig S5C). GSH is the major cellular redox buffer in eukaryotes [36]. For example under conditions of heat stress, GSH is known to react with proteins to form protein-S-SG disulfides, which protects the cell against damage from the formation of disulfide bridges between proteins [37]. Both GSH and GS-X are known to be actively exported from cells. For example, in higher eukaryotes, GSH is exported from the liver and transported to other organs via the blood stream, and GS-SG is exported for biliary excretion. Our results suggest that GS-X and GSH are likely released by live cells (Fig 2C; Fig S6), consistent with the ATP-dependent export of GSH and GS-X previously observed in yeast [16]. Furthermore, our data suggest that compared to GSH, GS-X might be preferentially exported (Fig 2C), consistent with cells purging unwanted GS-X. Our findings are consistent with previous observations that yeast upregulated glutathione transporters such as Gex1 and excreted GSH and GS-X [38] in response to cadmium-induced redox stress, and that Opt1, an oligopeptide transporter shown to export GSH [39], was upregulated in response to different environmental stressors [40,41].

Evolution of auxotrophy has been experimentally observed in previous work. At a high mutation rate (e.g. a high loss rate of plasmids that carry biosynthetic genes), auxotrophs could rise to a detectable level [42] possibly due to mutation-selection balance. When nutrients were supplied by either the medium or other microbes, initially rare auxotrophic mutants could rise to a detectable frequency due to their fitness advantages over their non-auxotrophic counterparts [18,19,43,44]. In the "energy saving" hypothesis, this fitness advantage is thought to be due to auxotrophs saving the energy of synthesizing the essential nutrient [18]. Contrary to the energy-saving hypothesis, the fitness advantage of *lys*$^-$*orgS*$^-$ over *lys*$^-$ was abolished when excess GSH was supplemented (Fig 4; Fig S8). Instead, the fitness advantage of *orgS*- was only present when organosulfurs were present at a low level. Limited organosulfurs, by mimicking natural sulfur limitation and shutting down the inappropriately active growth in *lys*$^-$*orgS*$^-$, could allow these cells to survive lysine limitation better than *lys*$^-$ (Fig 4).

In summary, lysine-limited *lys*$^-$ cells release organosulfurs. These organosulfurs at low levels not only support the growth of rare *lys*$^-$*orgS*$^-$ mutants, but also restore their growth regulation by imposing natural limitation. Consequently, *lys*$^-$*orgS*$^-$ gain an advantage over *lys*$^-$ and rise in frequency up to a steady-state value (Fig 4). Interestingly, nutrient-growth imbalance has been implicated in certain cancers [9]. Thus, understanding the evolutionary and ecological consequences of nutrient-growth imbalance in mammalian cells could be fruitful.

Acknowledgements
We thank Maxine Linial, Shannon Murray, and Linda Breeden for critically reading the manuscript.

Methods

Medium and strains
All strains used in this study are listed in Table S1. All yeast nomenclature follows the standard convention. For all experiments, frozen yeast strains stored at -80°C were first struck onto YPD (10 g/L yeast extract, 20 g/L peptone, 20 g/L glucose) + 2% agar plates and grown at 30°C for ~48 hours, from which a single colony was inoculated into 3 mL of YPD and grown overnight at 30°C with agitation. All experiments were carried out within 3 days of generating the overnight culture. Minimal medium (SD) contained 6.7 g/L Difco Yeast Nitrogen Base w/o amino acids w/ ammonium sulfate and 20 g/L D-glucose, except during glucose-limitation experiments where lower levels of glucose were used as specified. Depending on strain auxotrophy, SD was supplemented with lysine (164.3 µM), adenine sulfate (108.6 µM) [45], or organosulfurs (134 µM) so that cells could grow exponentially.

Evolution
Coculture evolution was described in an earlier study [12]. To revive a coculture, ~20 µL was scooped from the frozen sample using a sterile metal spatula, diluted ~10-fold into SD, and allowed to grow to moderate turbidity for 1-2 days. The coculture was further expanded by adding 3 mL of SD. *lys*- evolved clones were isolated by plating the coculture on rich media (YPD) agar with Hygromycin B.

For monoculture evolution, chemostat vessels (Fig S10) were placed into a core manifold with six receptacles, each with a magnetic stirrer. Reactor vessels were immobilized in receptacles by adjustable compression rings. A rubber stopper equipped with an inflow tube and a sampling needle covered the top of the vessel. Waste flowed by gravity to a waste receptacle below the device through C-Flex 0.375” ID tubing (Cole Parmer) attached to the outflow arm. Nutrient media was fed to the vessels from media reservoirs by tubing passed through a Cole Parmer MasterFlex C/L peristaltic pump controlled by a custom LabView console through a custom relay box. Media reservoirs were 1 L glass bottles capped with one-hole rubber stoppers. Tubing was fed through the stopper and allowed to hang to the bottom of the reservoir. The reservoirs were placed on Denver Instrument XP-1500 digital balances, and the actual flow rate for each vessel was determined from the rate of mass loss of the corresponding reservoir.

To create a sterile environment, initial assembly was done in autoclave trays, with vessels held in tube racks. Six reservoirs were prepared by adding 810 mL water to each bottle. Six vessels were prepared by adding a 10 mm stir bar and 20 mL growth media (SD+21 µM lysine) to each vessel. Media delivery tubing was attached between reservoirs and vessels through rubber stoppers, and waste tubing was attached to each outflow arm, with the unattached end covered by foil held in place by autoclave tape. A 1.5 mL micro-centrifuge tube was placed over the sampling needle and held in place by autoclave tape. Tubing ports were wrapped with foil as well. Each reservoir with its attached tubing was weighed, the entire assembly autoclaved, then each reservoir weighed again. Lost water was calculated and added back. Under sterile conditions, 90 mL of 10X SD and a lysine stock were added to each reservoir to reach a final lysine concentration of 21 µM. The vessels were then secured into the chemostat manifold receptacles, reservoirs placed on the scales, and tubing threaded into the pumps.

Ancestral or evolved *lys*- clones were grown in 50 mL SD + 164 µM lysine for ~20 hours prior to inoculation. Before each experiment, growth was tracked to ensure cells were growing optimally (~1.6 hour doubling time). When cells reached a density of ~0.2 OD600, cells were washed 3 times in SD and inoculated in a chemostat vessel prefilled with SD + 21 µM lysine. After this step, chemostat pumps were turned on at a set doubling time in the custom written LabView software package. Each chemostat vessel contained ~43 mL running volume, and was set to a target doubling time (e.g. for 7 hour doubling, flow rate is 43*ln2/7=~4.25 mL/hr). With 21 µM lysine in the reservoir, the target steady-state cell density was $7x10^6$/ mL. In reality, live cell densities varied between $4x10^6$/ml and $1.2x10^7$/ml. Periodically, 4 mL of supernatant was harvested and dispensed into a sterile 15 mL conical tube. Next, 300 µL of this cell sample was removed and kept on ice for flow cytometry analysis. The remaining 3.7 mL of supernatant was filtered through a 0.22 µM nylon filter into 500 µL aliquots and frozen at -80C. Each chemostat was sampled according to a pre-set sequence. For experiments with metabolite extraction, the chemostat vessel stopper was removed and cells from 20 mL of sample was harvested. Due to the breaking of vessel sterility, this would mark the end of the chemostat experiment.

The nutrient reservoir was refilled when necessary by injecting media through a sterile 0.2 micron filter through a 60 mL syringe. To take samples sterilely, the covering tube on the sampling needle was carefully lifted, and a sterile 5 mL -syringe was attached to the needle. The needle was then wiped with 95% ethanol, and slowly pushed down so that the tip was at least ~10 mm below the liquid level. A 5 mL sample was drawn into the syringe, the needle pulled up above the liquid surface, and an additional 1 mL of air drawn through to clear the needle of liquid residue. The syringe was then detached and the cap placed back on the needle. The samples were ejected into sterile 13 mm culture tubes for freezing and flow cytometry determination of live cell densities. In both evolution experiments, samples were frozen in 1 part 20% trehalose in 50mM sodium phosphate buffer pH 6.0 + 1 part YPD. The samples were cooled at 4°C for 15 min before frozen down at -80°C.

Whole-genome sequencing and data analysis are described in detail in [12].

Quantifying auxotroph frequency

Frozen cultures (2 time points from three mono-culture evolution and three co-culture evolution experiments) were revived, and clones were isolated and screened for auxotrophy. We revived frozen samples by directly plating samples on YPD (monoculture) or YPD + hygromycin (cocultures to select against the partner strain). Plates were grown at 30°C for 2~4 days until all colonies were easily visible for picking. We observed a variety of colony sizes, and screened both large and small sized colonies when both were present. We counted large and small colonies to estimate the ratio of large:small colony-forming cells in the population, then multiplied this fraction by the fraction of auxotrophs observed in each colony size class to get a full population auxotroph frequency estimate. To screen for auxotrophy, entire colonies were inoculated into 150 µl of SD, 10 µl of which was diluted into 150 µl SD in microtiter plates and incubated overnight to deplete organosulfur carry-over or cellular organosulfur storage. In the case of some small colonies, no dilution was made as the inoculated cell density was already low enough, based on OD measurements. 10-30 µl were then diluted into a final volume of 150 µl each of SD+Lys, SD+Lys+Met, and YPD, aiming for OD~0.005-0.03 based off an initial reading by a 96-well plate OD600 reading of the starvation plate. Plates were then incubated for 48+ hours to grow cultures to saturation, and culture turbidity (OD600) was read using a 96-well plate reader. Control wells

of known *lys*$^-$*orgS*$^-$ (WY1604) and *lys*$^-$ (WY2226) were included in the screening as controls. Wells that grew in SD+Lys+Met and YPD but failed to grow in SD+Lys were scored as *lys*$^-$*orgS*$^-$.

Fluorescence microscopy

Fluorescence microscopy experiments and data analysis are described in detail elsewhere [46]. Briefly, the microscope is connected to a cooled CCD camera for fluorescence and transmitted light imaging. The microscope harbors a temperature-controlled chamber set to 30°C. The microscope is equipped with motorized switchable filter cubes capable of detecting a variety of fluorophores. It also has motorized stages to allow z-autofocusing and systematic xy-scanning of locations in microplate wells. Image acquisition is done with an in-house LabVIEW program, incorporating autofocusing in bright field and automatic exposure adjustment during fluorescence imaging to avoid saturation. Previous analysis [46] has demonstrated that background-subtracted fluorescence intensity scales proportionally with live cell density, and a decrease in fluorescence intensity correlates well with cell death.

For experiments in Fig 1, WY2490 (*lys*-) was grown overnight to exponential phase in SD+164 µM lysine, washed 3 times in SD, and starved for 3 hours at 30 ^{o}C in a never-used 13 mm test tube in SD. Then, the cells were harvested, washed 3 times with YNB (SD without glucose), and starved for 3 days at 30°C (this is to ensure that cells are truly starved for glucose and would not keep growing in the absence of glucose under microscope). For experiments in Fig 5, cells were grown overnight to exponential phase, washed 3 times in SD, and starved for 24 hours at 30 ^{o}C In a 96 well plate with either YNB, YNB+2% glucose (SD), or SD+1 µM rapamycin, ~10,000 cells/well were inoculated and mCherry intensity over time was collected. The microtiter plate was imaged periodically (1~2 hrs) under a 10x objective in a Nikon Eclipse TE-2000U inverted fluorescence microscope using an ET DsRed filter cube (Exciter: ET545/30x, Emitter: ET620/60m, Dichroic: T570LP).

Chemostats and turbidostats

Cells were grown under controlled conditions using a custom-made continuous culturing device (Fig S10A), with six channels (Fig S10C) where each can be independently operated as a chemostat or a turbidostat. When operated as a chemostat, a channel provides a limited nutrient environment where the growth rate is held constant. When operated as a turbidostat, a channel maintains a constant cell density while cells grow with an abundant supply of nutrients.

The continuous culturing device consisted of six reactor vessels (Fig S10A), each with a volume of ~43ml determined by the height of the outflow tube (Fig S10C, E). A rubber stopper equipped with an inflow tube and a sampling needle covered the top of each vessel (Fig S10C). The vessels were placed in an aluminum mounting frame with six receptacles (Fig S10A, back), each equipped with an integrated magnetic stirrer (made from a CPU fan, magnets, and 3D printed clip) and an LED-phototransistor optical detector for OD measurements. The vessels were immobilized in the receptacles by adjustable compression rings. A sampling needle passed through a seal provided by a short length of glass tubing, so that sampling needle could be easily lowered into the reactor for sampling and elevated above the culture level when not sampling. The tightness of the seal was adjusted by application of zip-ties to the end of glass tubing with the proper tightness to allow movement yet with enough friction to maintain position. Waste flowed by gravity to a waste receptacle below the device through 0.375” ID tubing (Cole Parmer C-Flex) attached to the outflow arm. Nutrient media was fed to each vessel from an independent reservoir by a peristaltic pump (Welco WPM1, operated at 7V DC). The media delivery tube consisted of two

sections of generic 2mm OD, 1mm ID PTFE tubing, joined by insertion into the two ends of a 17cm section of PharMed AY242409 tubing (Saint-Gobain) which was inserted into the peristaltic pump (Fig S10B). The pump was activated and deactivated by the custom LabView program through a relay box (Pencom Design, Inc. UB-RLY-ISO-EXT-LR). Depending on whether a given channel was in chemostat or turbidostat mode, the LabView program controlled pump in different ways (i.e. constant dilution rate in chemostat, or dilution to a set turbidity in turbidostat). Data for OD and flow rate data were logged in either mode of operation. In both cases, flow rate can be used to calculate growth rate. Media reservoirs (Fig S10A front) were 1 L glass bottles capped with one-hole rubber stoppers, and a section of glass tubing was used as a sleeve to prevent curling of the PTFE tubing and to keep the end of PTFE tubing touching the bottom of the reservoir. Each reservoir was placed on a digital balance (Ohaus SPX2201) with a digital interface (Ohaus Scout RS232 interface) for measurement of the volume (weight) remaining in the reservoir at any given time.

When in turbidostat mode, constant average turbidity was maintained. Specifically, the pump was activated when the measured OD was above the set point and deactivated when the OD was below set point. OD was measured using an 940nm LED (Ledtecch UT188X-81-940, driven with 50ma current) and phototransistor (Ledtech LT959X-91-0125). Each LED-phototransistor pair was tested and selected for consistent OD measurements. The LED and phototransistor were positioned by mounting holes on the aluminum metal frame, on opposite sides of the reactor vessel, 4 cm from the vessel bottom. Each phototransistor was connected to an op-amp (LM324) circuit that acted as a current to voltage converter and buffer (Fig S10B). An isolated DC-DC converter provided a regulated voltage supply for the electronics. The output voltage from the photodetector circuit was digitized using a DAQ (National Instruments USB-6009), and read by the LabView program for OD measurement. The Labview program stored the average light intensity I_0 over the first two minutes after starting a channel as the "blank" value. The light intensity, I, was measured every ~30s, and the OD = $\log_{10}(I/I_0)$ was calculated.

When in chemostat mode, a constant average flow rate *f* of medium into the vessel was maintained. Unlike our earlier chemostat setup [47], here constant flow rate was achieved via a scale (Ohaus SPX2201) which constantly weighed its associated reservoir, and the reading was acquired through an RS232 interface (Ohaus Scout RS232). The initial scale reading, $M_{initial}$, was recorded when the chemostat channel was activated or reset. This was used with the current scale reading $M_{current}$ to calculate the total volume pumped from the reservoir to the vessel as $1ml/g * (M_{current} - M_{initial})$. The target volume that should have flown from the reservoir to the vessel at the current time was calculated according to the pre-set flow rate. If the total volume was less than the target, the pump was activated, and otherwise, the pump was deactivated. This provided the correct average flow rate. The flow rate was chosen for the desired doubling time, $f = ln(2) * V / T_D$, where V is the volume of the vessel and T_D the doubling time. Vessel volumes were measured by weighing empty vessel, and then weighed again when filled to the spillover point (Fig S10E), giving an average value of 43ml. Individual flow rates were determined using individual vessel volumes. Volume measurements are limited by the minimum waste tube drop size of ~0.5 ml, which is constrained by surface tension. Scale readings were logged, providing a measure of flow rate (Fig S10D).

Bioassays

Most bioassays are yield-based. Various tester strains were used in this study (specified in each experiment; Table S1), but preparation for all yield-based bioassays was the same. Strains were grown for

~16 hours in SD and any required supplements. During this time, growth rate was tracked to ensure cells were doubling as expected (1.6 to 3 hour doubling depending on the strain/condition). After this time, cells were washed 3 times with 3 mL SD and starved for at least 3 hours at 30°C in 3 mL SD in a never used 13 mm test tube (to prevent inadvertent nutrient contamination). This was done to deplete cells of vacuolar stores of nutrients. Finally, ~1000 cells/well were inoculated into a final volume of 150 µL into a flat-bottomed 96 well plate of either metabolite standards or supernatants, supplemented with SD+1x lysine. For each auxotrophic strain, SD+1x lysine supplemented with various known concentrations glutathione were used to establish a standard curve that related organosulfur concentration (in terms of fmole GSH equivalent) to final turbidity (Fig S4). Turbidity achieved in a supernatant was then used to infer organosulfur concentration in the supernatant. Plates were wrapped with parafilm to prevent evaporation and incubated at 30˚C for 2 days. We re-suspended cells using a Thermo Scientific Teleshake (setting #5 for ~1 min) and read culture turbidity using a BioTek Synergy MX plate reader.
In a rate-based bioassay (Fig S3B), mCherry tagged yeast strain auxotrophic for organosulfur (WY2035) was pre-grown in SD +164 µM Lys +134 µM Met and growth rate was tracked by optical density to ensure the cell was growing as expected. Next, cells were washed 3 times in SD lacking supplements, and starved for at least 3 hours in never-used 13 mm test tubes (to prevent nutrient contamination). Cell density was measured again by OD, and cells were inoculated to roughly 1000 cells /well in a 96 well plate in a total volume of 300 µL. The well was filled with either known quantities of organosulfur (methionine or glutathione) or harvested supernatants, both supplemented into SD + 164 µM lysine. The 96 well plate was measured in the same manner as previously outlined in the "Fluorescence microscopy" section.

Maximal grow rate was calculated by measuring the slope of ln(Normalized Intensity) against time. For each sliding window of 4 time points, slope is calculated and if it exceeds the current max slope for the well, it is chosen as the new maximum. To ensure that no estimation occurs when other metabolites, such as glucose, could be limiting, we restricted analysis to data at 25% maximal intensity to ensure that cells had at least 2 doublings beyond when they are theoretically growing maximally. For this study, maximal growth rates were used to estimate approximate niche size, the logic being that cells should grow faster if there is a larger organosulfur niche.

Flow cytometry

Detailed description can be found elsewhere [48]. Population compositions were measured by flow cytometry using a DxP10 (Cytek). Fluorescent beads of known concentration (as determined by hemocytometer) were added to determine cell densities. A final 1:20,000 dilution of ToPro3 (Molecular Probes T-3605) was used for each sample to determine live and dead cell densities. Analysis using FlowJo software showed obvious clustering of live and dead cells in the ToPro3 RedFL1 channel, with dead cells having a RedFL1 signal of $>10^3$. Dead cell densities typically were never higher than 10% in all conditions tested.

Metabolite extraction

Metabolite extraction for intracellular organosulfur quantification was adapted from [49]. Briefly, 20 mL of chemostat populations are harvested in disposable 25 mL pipettes, and rapidly vacuum filtered onto precut 0.45 µm Magna nylon filters (GVS Life Sciences, USA). Filters were then quickly submerged with ethanol cleaned forceps in into 3 mL ice-cold extraction buffer (held in a 5 mL sterile centrifuge tube) mixtures, which consisted of 40% (v/v) acetonitrile, 40% (v/v) methanol, and 20% (v/v) of distilled water. All reagents were HPLC grade and all extraction buffer mixtures were made fresh before each extraction. The centrifuge tube was capped and quickly vortexed to remove all cells. The entire process took less

than 25 seconds, with the time between populations being filtered and submerged in extraction buffer being less than 10 seconds. After all populations had been harvested, extracts were frozen at -80 ^{o}C until solid, transferred to ice and allowed to thaw. After the samples had thawed, they were incubated on ice for 10 minutes and vortexed once every ~3 minutes and returned to -80°C for refreezing (a single 'freeze-thaw' cycle). After 3 freeze-thaw cycles, 1.5 mL of sample was harvested and transferred to a new 1.5 mL micro-centrifuge tube, and centrifuged at 13,0000 rpm for 2 minutes at 4°C to pellet the cell debris. The extract was removed and the remaining cell pellet was extracted again with 1.5 mL of extraction mixture, and spun down. The final result was 3 mL of extracted metabolites that was stored at -80°C and analyzed by HPLC less than 48 hours after extraction. To check that a majority of metabolites were extracted, 100 µL of fresh extraction buffer was added to the collected cell debris, vortexed vigorously, and collected by centrifugation. This 100 µL 'second extract' was also analyzed for glutathione by HPLC. On average, the amount of glutathione in the second extract was < 2% of the amount extracted initially in the 3 mL extraction.

Analytical chemistry quantification of glutathione (GSH) and glutathione S-conjugates (GS-X).

HPLC

Reduced glutathione was derivatized using a thiol-specific probe first described by [50], called Thiol Probe IV (EMD Millipore) to make a fluorescent glutathione conjugate. The compound reacts readily with free-thiols, though at different rates. For quantifying glutathione, 270 µL of sample or GSH standard in SD was added to 30 µL of 833 mM HEPES buffer, pH 7.8. This was done to raise the pH of the sample to a basic level, which facilitates the reaction. Next, the probe (dissolved in DMSO and stored in 50 µL aliquots at -20 C), was added to a final concentration of 100 µM, which is in excess of glutathione by at least 10-fold. The reaction was performed at room temperature in the dark (the probe is light-sensitive) in a 96-well plate for 20 minutes. After this, 8.4 µL of 2M HCl was added to rapidly quench the reaction by lowering the pH to ~2. This also stabilizes the fluorescent conjugate. The entire sample was then added to a 250 µL small volume pulled point class insert (Agilent Part No: 5183-2085) to facilitate autosampler needle access. The small volume insert with sample was then placed inside a dark-brown 1.5 mL autosampler vial (Shimadzu Part No: 228-45450-91) and capped with a fresh 9mm screw cap with PTFE septum (Shimadzu Part No: 228-45454-91).

Derivatized glutathione was separated and identified using reverse phase chromatography. 10 µL of the reaction mixture was injected onto Synergi 4 µM Hydro-RP 80 Å LC Column 150 x 4.6 mm (Phenomenex, Part No: 00F-4375-E0) fitted with a SecurityGuard Cartridges AQ C18 4 x 3.00 mm ID (Phenomenex, Part No: AJO-7511) in a SecuirtyGuard Cartridge Holder (Phenomenex, Part No: KJ0-4282). The SecurityGuard (pre-column) was periodically replaced whenever pressure reading exceeded the manufacturer's specifications. Glutathione was eluted from the column with a mobile phase gradient of filtered Millipore water (Solution A) and acetonitrile (Solution B, HPLC grade). The Millipore water was filtered through a 0.22 µM filter prior to use. Additionally, before each run the column was equilibrated for 30 minutes with 1% Solution B. The % solution B followed the following program for each injection: 0 min 1%, 10 min 14%, 10.01 min 1%, and 15 min 1%, corresponding to a gradual increase to 14% Solution B over 10 minutes, followed by a re-equilibration with 1% Solution B. The column was maintained at a running temperature of 25 ^{o}C in a Nexera X2 CTO-20A oven. Flow rate was 1 mL /min. Under these conditions, glutathione eluted at ~ 7 minutes, with slight run-to-run variation. Fluorescent glutathione was detected by excitation at 400 nm and emission at 465 nm. After each run, the column was washed and stored per manufacturer's instructions.

Analysis of HPLC data was done using the R Statistical Language with custom written software for peak-picking, baseline correction, plotting, and area estimation, which is freely available at https://bitbucket.org/robingreen525/hplc_rscripts/src/master/ . Raw data for each sample run was exported to a text file and parsed in the RStudio environment. Emission data (at 465 nm) was culled to restrict analysis from 6.5 to 8 minutes. Next, the script identified a local maximal peak, which for concentrations above 0.01 µM glutathione always corresponding to glutathione. Anything lower was indistinguishable from the background. Next, the script identified local minima on both sides of the glutathione peak and drew a baseline that connected the two. The formula (y=mx+b) for this line was calculated and the baseline was 'corrected' by subtracting the emission spectrum value for each point against the y value of the calculated formula for the same point. To quantify the concentration of glutathione in a sample, known concentrations of GSH in SD were subjected to the above procedure. A standard curve of 0.03 to 1 µM was typically used and showed little variability between experiments. An example of these data are shown in Figure 2A. A linear regression model of peak area against concentration of reduced glutathione was built using the lm function of the stats package. Samples with areas within the dynamic range (0.03-1 µM GSH) were back-calculated using the linear regression model. Comparing HPLC traces of the same derivatized sample over 24 hours shows that glutathione peak area is within 10% of all replicates.

LC-MS

Supernatants were shipped over-night on dry ice to the Rabinowitz lab at Princeton University. Stable isotope compound [2-^{13}C, ^{15}N] Glutathione (GSH) was obtained from Cambridge Isotope Laboratories. HPLC-grade water, methanol, and acetonitrile were obtained from ThermoFisher Scientific. Supernatant sample was thawed at room temperature and 30 µL of the supernatant together with 5 µL of 10 µM 2-^{13}C+^{15}N labeled GSH was transferred into a 1.5 mL centrifuge tube. The samples were either run directly to measure GSH only, or first treated with TCEP to reduce GS-X to GSH and then measure the total GSH. For those samples with TCEP treatment, 5 µL of 60 g/L tris(2-carboxyethyl)phosphine solution (TCEP, reducing reagent) was added into the sample. The resulting mixture was vortexed and incubated for 20 min at room temperature. Afterward, 10 µL of 15% NH_4HCO_3 (w/v) was introduced to neutralize the pH of the solvent. The solution was dried down under N_2 flow and resuspended in 50 µL 40:40:20 (methanol/acetonitrile/water) solvent and kept at 4 °C in an autosampler.

Samples were analyzed using a Q Exactive Plus mass spectrometer coupled to Vanquish UHPLC system (Thermo Scientific). LC separation was achieved using a XBridge BEH Amide column (2.1 mm x 150 mm, 2.5 µm particle size, 130 Å pore size; Waters, Milford, MA) using a gradient of solvent A (20 mM ammonium acetate + 20mM ammonium hydroxide in 95:5 water: acetonitrile, pH 9.45) and solvent B (acetonitrile). Flow rate was 150 µl/min. The gradient was: 0 min, 90% B; 2 min, 90% B; 5 min, 50% B; 10 min, 0% B; 13.5 min, 0% B; 15 min, 90% B; 20 min, 90% B. Column temperature is 25˚C and injection volume is 10 µL. Mass spectrometer parameters are: positive ion mode, resolution 140,000 at m/z 200, scan range m/z 290-650, AGC target 3E6, Maximum injection time 200 ms. Quantitation of Glutathione concentrations in samples were achieved by comparing the peak areas of glutathione to those of ^{13}C-GSH. Data were analyzed using the MAVEN software[51].

Distinguishing live versus dead release and calculating release rate

To calculate the amount of glutathione each dead cell would need to release for the total pool of glutathione to be explained by cell lysis alone (the 'dead release' model), concentration of supernatant glutathione (in µM) was divided by dead cell density (cell/ mL) as determined by TO-PRO straining (See

Flow Cytometry section). This number was multiplied by $1x10^6$ to get fmole/dead cell, the amount each dead cell would need to have inside it to explain the total pool of glutathione by cell lysis alone. This method has previously been described by [52].

To calculate the release rate of glutathione per live cell in chemostats, we used a previously described method [48]. Briefly, steady state concentration of glutathione in chemostat was divided by live cell density as determined by TO-PRO straining, and multiplied by dilution rate (/hr),

Competition

To quantify multiple competition replicates at multiple initial strain ratios, we used the coculture system to mimic the lysine-limited environment, especially since similar mutations in coculture and monoculture lysine-limited chemostats meant that the environments were similar. To do so, WY1340 (the purine requiring/lysine releasing strain in the RM11 background) was grown to exponential phase overnight in SD+134 µM adenine, washed 3 times with SD to remove adenine, and starved for 24 hours to deplete vacuolar storage. During this starvation, WY2702/2073 (BFP *met10* evolved clones) and WY2429 (mCherry *MET10* evolved clone) was grown overnight in SD + 134 µM methionine to exponential phase, washed 3 times, washed 3 times with SD to remove excess methionine and lysine. Next, WY2072/3 and WY2429 were mixed in ratios of 1:100, 1:10, 1:1, and 10:1 to a final OD_{600} of 0.1. This mixture of populations was then added 1:1 with WY1340 to a final OD_{600} of 0.03. This was considered generation 0. Populations were monitored for growth by measuring optical density over time and periodically diluted back to OD600 0.03 (OD_{600} was never greater than 0.45 to ensure no additional metabolites from SD was limiting). The OD_{600} data was used to back calculate total generations in the experiment. Periodically, 100 µL of the culture was sampled for flow cytometry to track strain ratios. Experiments were performed until the strain ratio stabilized.

The steady state species ratio may be estimated in the following fashion. At steady state species ratio, organosulfur releasers and consumers grow at an identical rate, and organosulfur concentration is in steady state. From 8-hr doubling time chemostat experiment (Fig 3), the steady state concentration of organosulfurs was 1.4~1.5 µM GSH equivalent, and the steady state live population size was $4.6\sim4.8x10^6$/ml. Thus, the release rate was ~0.026 fmole GSH equivalent/cell/hr. From Fig S4 and since in our setup 1 OD~ $3x10^7$ cells/ml, organosulfur consumption per birth during starvation was 2.1 fmole GSH/cell. The organosulfur concentration *O* at steady state can be described as:

$$\frac{dO}{dt} = rR - cgC$$

where *R* and *C* are the concentrations of releaser and consumer cells, respectively, and *g*, *r*, and *c* represent growth rate (equal dilution rate in chemostats), release rate of organosulfurs, and organosulfur consumption amount per birth, respectively. Setting this to zero, and we obtain:

$$\frac{C}{R} = \frac{r}{cg} = \frac{0.026\, fmole / cell / hr}{2.1\, fmole / cell * \ln(2) / 8hr} = 0.14$$

. This is consistent with Fig 4 where the steady state ratio of consumer to releaser was ~0.1. Note that here we assumed that all organosulfur compounds can be considered as GSH equivalents.

Figures

Fig 1. Evolution of organosulfur auxotrophy in cells suffering nutrient-growth imbalance.

Fig 1 (**A**) *lys*- cells suffer nutrient-growth imbalance when limited for lysine but not when limited for glucose. Exponentially-growing mCherry-expressing *lys*- (WY2490) cells were washed and starved for lysine and glucose to deplete cellular storage, and cultured and imaged in indicated environments. Total fluorescence serves as an indicator of total live biomass, increasing if cells grow in size or give birth to new cells, and decreasing if cells die [48]. In the absence of lysine, *lys*- cells died rapidly when glucose was abundant (2%, "Excess C", dark blue circles), and rapid death could be rescued by the TORC1 inhibitor rapamycin (1 μM, blue crosses). *lys*- cells survived well when the medium lacked glucose in addition to lacking lysine ("No C", green circles). These observations are consistent with the following model: In abundant natural nutrients without lysine, cells attempt to grow, leading to cell death (iii). When carbon is missing (ii) or when rapamycin is applied to inhibit TORC1 (i), cells stop growth, engage in starvation-responsive program, and survive lysine limitation. Total fluorescence intensity is normalized to the initial value, and error bars correspond to 2 standard deviations for 5 replicate wells. (**B**) The emergence of *lys*$^-$ *orgS*$^-$ auxotrophs. *lys*- cells (WY950 or WY1335) were grown for tens of generations in minimal medium SD containing limiting lysine and no other amino acids, either in lysine-limited chemostats [53] or via co-culturing with a lysine releaser in a cross-feeding yeast community [48,54]. Out of 20 independent lines, we randomly isolated ~70 clones for whole-genome sequencing. Chemostat evolution and coculture evolution both yielded *met*- mutants (1 out of 9 clones in chemostat evolution; 3 out of ~60 clones in coculture evolution). These mutants required an externally-supplied organosulfur such as methionine to grow. In the experiment shown here, clones were grown to exponential phase in SD supplemented with amino acids, washed with SD, starved for 3 hours to deplete cellular storage, and spotted on indicated agar plates for 2 days at 30°C.

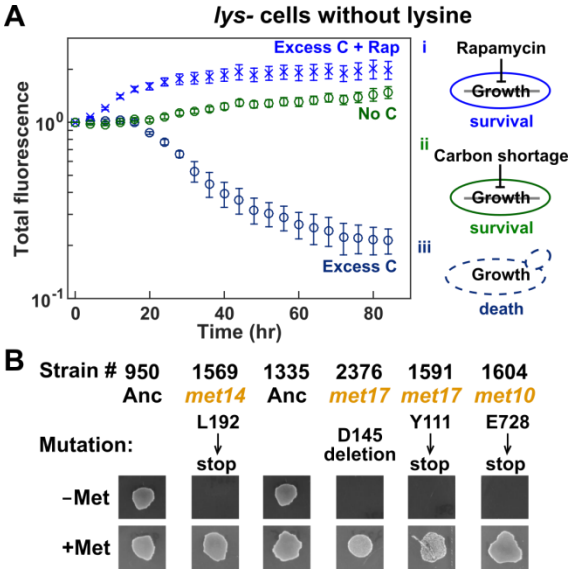

Fig 2. Lysine-limited live *lys*- cells mainly release glutathione (GSH) and glutathione S-conjugates (GS-X).

Fig 2 (**A**) Mass spectra traces of reduced glutathione (GSH) ion. Gray and black lines correspond to known quantities of GSH in growth media. Blue and green correspond to filtered supernatants of ancestral *lys*$^-$ cells (WY1335) growing in lysine-limited chemostats at indicated doubling time. Supernatants were harvested at ~48 hrs. (**B**) GSH and GSH S-conjugates (GS-X) constitute the majority of the organosulfur niche. Supernatants of *lys*- cells (WY1335) growing in lysine-limited chemostats (8-hr doubling) were harvested at steady state (~26 hr) and filtered. (**i**) Bioassay quantification of the total organosulfur niche. Quantification was performed by comparing the final turbidity of *met10*- (which can grow on a variety of organosulfurs including methionine, GSH, and GSX; Fig S4) grown in supernatants versus in various known concentrations of GSH. (**ii, iii**) GSH in supernatant was quantified by HPLC and LC-MS. (**iv**) GSH+GS-X in supernatants were quantified by reducing GS-X with TCEP and measuring total GSH via LC-MS (Methods). Error bars mark two standard deviations of samples from three independent chemostats. (**C**) Organosulfurs are likely released by live cells. Ancestral *lys*- cells (WY1335) were cultured in lysine-limited chemostats (doubling time 8 hrs). Total organosulfur in chemostat supernatant (brown) far exceeded that released by dead cells (purple). We quantified supernatant organosulfurs using a *met10* turbidity-based bioassay. To quantify dead cell release, we measured dead cell density using flow cytometry (Methods, 'Flow cytometry'), and multiplied it with the average amount of organosulfur per cell using a *met10* turbidity-based bioassay (Methods, 'Metabolite extraction'). Three independent experiments are plotted.

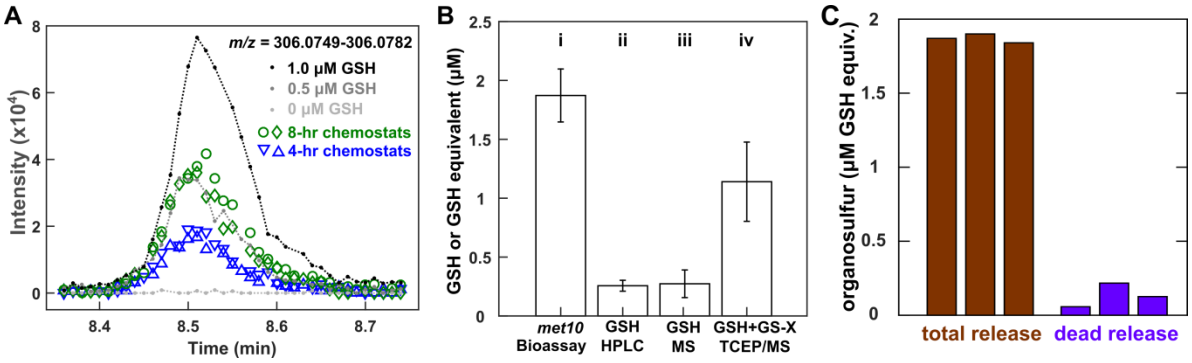

Fig 3. Organosulfurs release is associated with nutrient-growth imbalance.

Fig 3 *lys*- cells (WY1335) release organosulfurs when suffering from imbalanced growth in lysine-limited chemostats, but not in carbon-limited chemostats where growth is better tuned to nutrient availability. All chemostats with indicated input medium were run at 8-hr doubling time. (**A**) Higher percent dead cells in lysine-limited chemostats than in glucose-limited chemostats. Live and dead cell densities were measured via flow cytometry (Methods, "Flow cytometry"). (B) Higher organosulfur concentrations in lysine-limited chemostats than in glucose-limited chemostats. Organosulfur concentration was measured in terms of GSH equivalents using a *met10*- turbidity-based bioassay (Fig S4C), with brown dotted line marking the lower limit of the linear detection range.

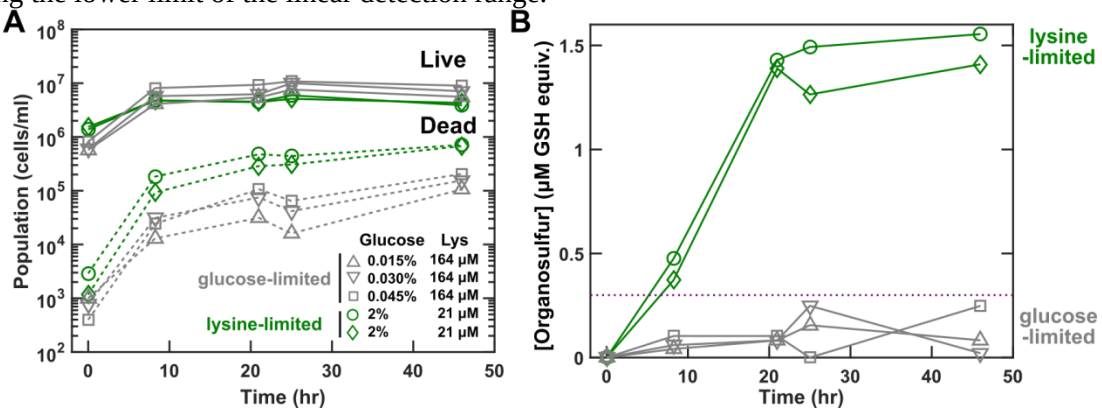

Fig 4. Restored nutrient-growth balance confers *lys⁻orgS⁻* a negative frequency-dependent fitness advantage over *lys⁻* during lysine limitation.

Fig 4 (**A**) **Fitness advantage of *lys⁻orgS⁻* over *lys⁻* requires low organosulfur and autophagy**. Cells were grown in excess nutrient (SD+164 µM lysine+134 µM GSH) to exponential phase, incubated in indicated environments in a 96-well plate and imaged (Methods, "Fluorescence microscopy"). Fluorescence intensities normalized against the initial value can be used to quantify live biomass [48]. (**Left**) In excess lysine and GSH, *lys⁻orgS⁻* (WY1604, orange) grows slower than *lys⁻* (WY2429, blue). (**Right**) When organosulfurs are limited, *lys⁻orgS⁻* survives lysine limitation better than *lys⁻* (yellow open circles above blue open circles). This survival advantage is diminished when GSH is abundant (yellow filled circles), which can be reversed by inhibiting growth-activator TORC1 via rapamycin (yellow crosses). Survival advantage conferred by growth down-regulation, through either organosulfur limitation or rapamycin, is abolished when autophagy is prevented (*lys⁻orgS⁻atg5⁻*; WY2370, green circles and crosses). Error bars represent two SEM (standard error of mean) from six wells. In (**B**), cells were washed and starved in SD for 24 hours prior to imaging in indicated conditions with (crosses) or without (circles) 1 µM rapamycin. The ~3-fold increase in fluorescence in (**B**) is due to cell swelling [48]. (**C**) Isogenic BFP-tagged *lys⁻orgS⁻* (WY2072 or WY2073) and mCherry-tagged *lys⁻* (WY2045) were competed in a lysine-limited environment by coculturing with a lysine-releasing strain (WY1340) (Methods). The ratio of *lys⁻orgS⁻* to *lys⁻* over time was measured by flow cytometry (Methods) over time. Both strains shared the identical evolved background harboring adaptive mutations including chromosome 14 duplication and *ecm21*. Smooth lines serve as visual guide. Different colors represent different starting ratios, while different symbols represent different experiments.

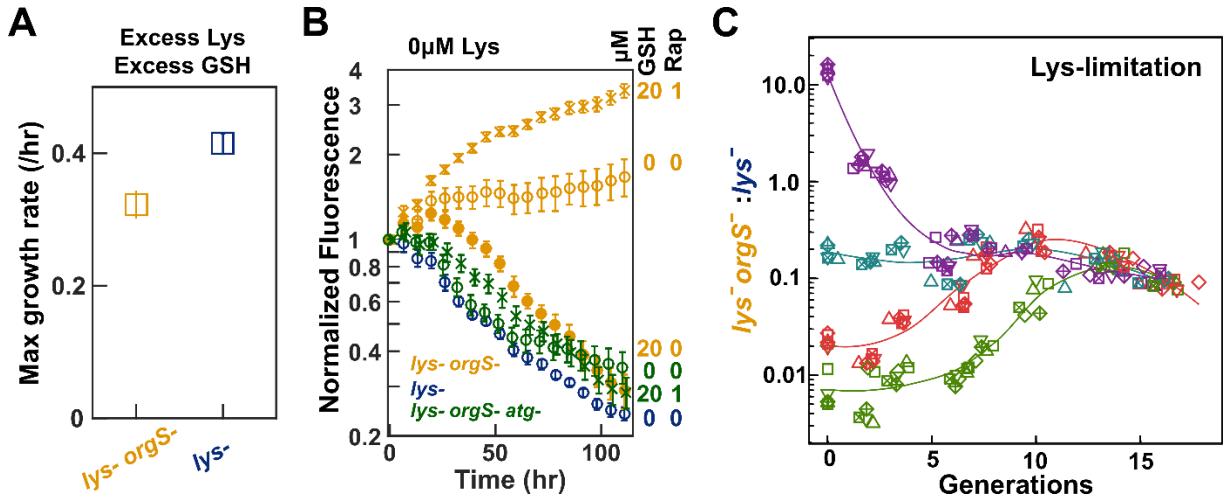

Fig S1. Organosulfur biosynthesis pathway in *S. cerevisiae*

Fig S1 Organosulfurs are organic compounds that contain sulfur. *S. cerevisiae* utilizes sulfate supplied in the medium to synthesize homocysteine, which is then used to make a variety of other organosulfur compounds (blue) including homocysteine, methionine, cysteine, and glutathione [55]. All *lys*$^-$*orgS*$^-$ mutants we have identified (orange) fail to synthesize homocysteine, and thus can be supported by any of the organosulfurs depicted here as well as potentially other organosulfurs.

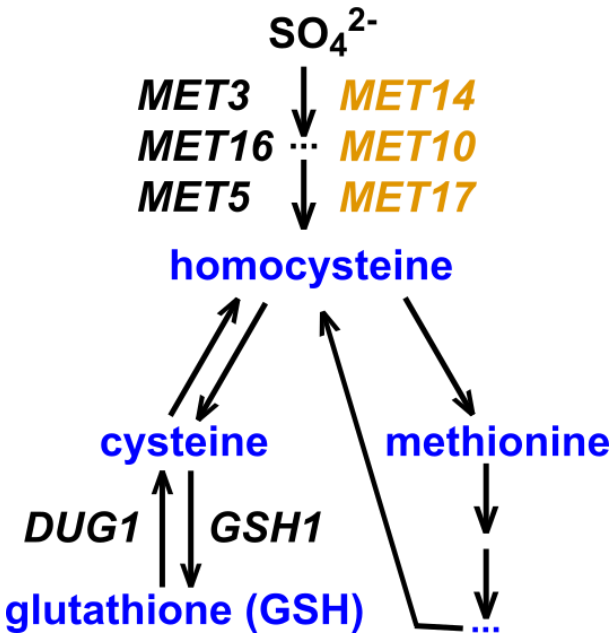

Fig S2. *lys*$^-$*orgS*$^-$ repeatedly rose to detectable frequency when *lys*- cells were limited for lysine

Fig S2 *lys*- cells (WY1335) were either cocultured (crosses) with a lysine-releasing strain (WY1340) or cultured alone in lysine-limited chemostats (circles). Cultures were frozen periodically in 50% trehalose. We revived frozen samples by directly plating samples on YPD or, in case of cocultures, YPD + hygromycin to select against the partner strain. We observed a variety of colony sizes, and since large and small colonies had different percentages of *lys*$^-$*orgS*$^-$, we quantified both types and calculated the overall *orgS*- in the population (Methods). Colonies that grew in YPD and SD+Lys+Met but failed to grow in SD+Lys were scored as *lys*$^-$*orgS*$^-$. Different colors indicate independent evolution lines. The fraction of *lys*$^-$*orgS*$^-$ is much lower in monocultures compared to cocultures. One possibility is that in coculture experiments, the lysine-releasing strain also released organosulfurs.

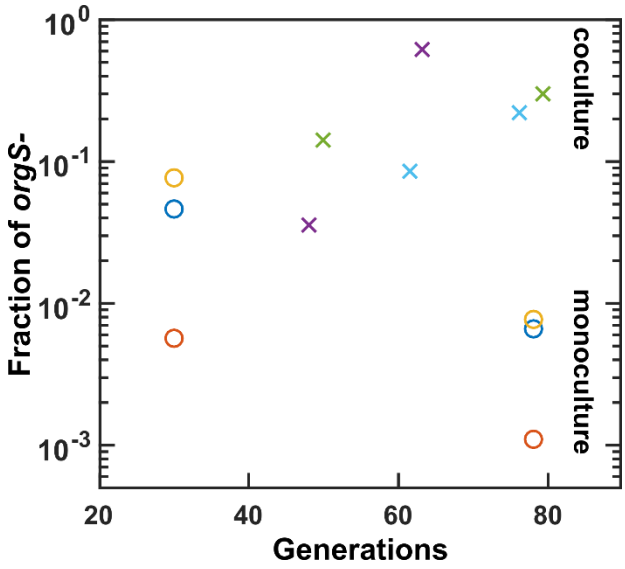

Fig S3. Rapid accumulation of organosulfurs upon lysine limitation

Fig S3 Ancestral *lys*- cells (WY1335) were grown to exponential phase in SD supplemented with excess lysine, washed free of lysine, and inoculated into replicate lysine-limited chemostats (different symbols) with 8-hr doubling time (green) or 4-hr doubling time (blue). Periodically, culture supernatants were quickly sampled, filtered, and frozen at -80°C to preserve the redox states of released compounds. (**A**) Population dynamics of live (fluorescent) and dead (non-fluorescent) cells in chemostats, as quantified by flow cytometry (Methods). (**B**) Organosulfurs in supernatants were measured as "methionine equivalents" by comparing growth rates of a *met17*- tester strain (WY2035) in supernatants fortified by SD versus in SD supplemented with known concentrations of methionine (standard curve in inset). Since the growth rate of tester cells can be affected by factors other than organosulfurs (e.g. pH), the organosulfur niche estimated by a rate-based bioassay can differ from that estimated from a turbidity-based bioassay (e.g. Fig 3B). Nevertheless, this assay motivated the LC-MS experiments that identified GSH as one of the released organosulfurs (Fig 2A). Specifically, the steady state concentration of a released chemical in a chemostat can be expressed as [release rate]*[live cell density]/[dilution rate] [48]. Thus, released chemicals should be twice as concentrated in 8-hr chemostats as in 4-hr chemostats due to the different dilution rates if all else are constant. In this experiment, although the steady state had not been reached by 72 hrs, organosulfurs in 8-hr chemostats were generally ~4-fold those in 4-hr chemostats, consistent with a faster organosulfur release rate in 8-hr chemostats than in 4-hr chemostats (**C**). Regardless, using liquid chromatography-mass spectrometry and the criterion that steady-state supernatants from 8-hr doubling time chemostats contained more organosulfurs than those from 4-hr doubling time chemostats, we identified glutathione as a released organosulfur (Fig 2A). (**C**) The release rate of organosulfurs is higher in 8-hr doubling chemostats compared to 4-hr doubling chemostats. Release rates were calculated from the first 24 hrs. A total of five replicates from two experiments are plotted. If organosulfurs are the major released compounds that affect *met17* growth rate, then release rates in 8-hr chemostats are significantly higher than in 4-hr chemostats by t-test.

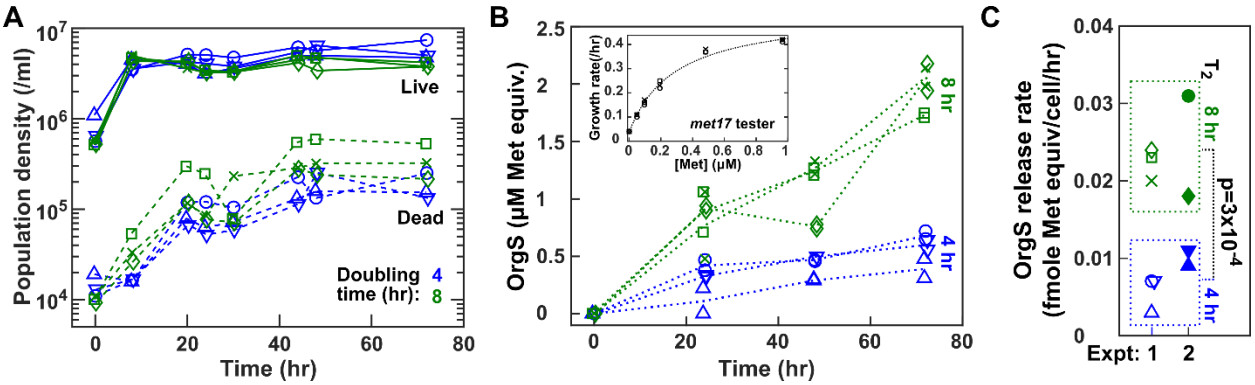

Fig S4. Turbidity-based bioassays of organosulfurs

Fig S4 (**A**) Sensitivity of turbidity (OD_{600}) measurements in a micro-titer plate. Purple dotted line marks the lower-bound of turbidity reading that we accepted as valid data, and is plotted in **B-D**. (**B**) The turbidity of a *gsh1*- strain (WY2509) increases linearly with [GSH] and [GSSG] within a range, but does not increase when supplemented with methionine. (**C, D**) *met10*- can use methionine, GSH, and oxidized glutathione (GSSG). For both *gsh1*- and *met10*- strains, since reduction of one GSSG molecule generates two GSH molecules, culture maximal turbidity in GSSG should be twice as much as in equal-molar GSH. This is indeed observed. (**E**) *gsh1*- and *met10*- grew to similar levels in supernatants of *lys*- cells grown in lysine-limited chemostats.

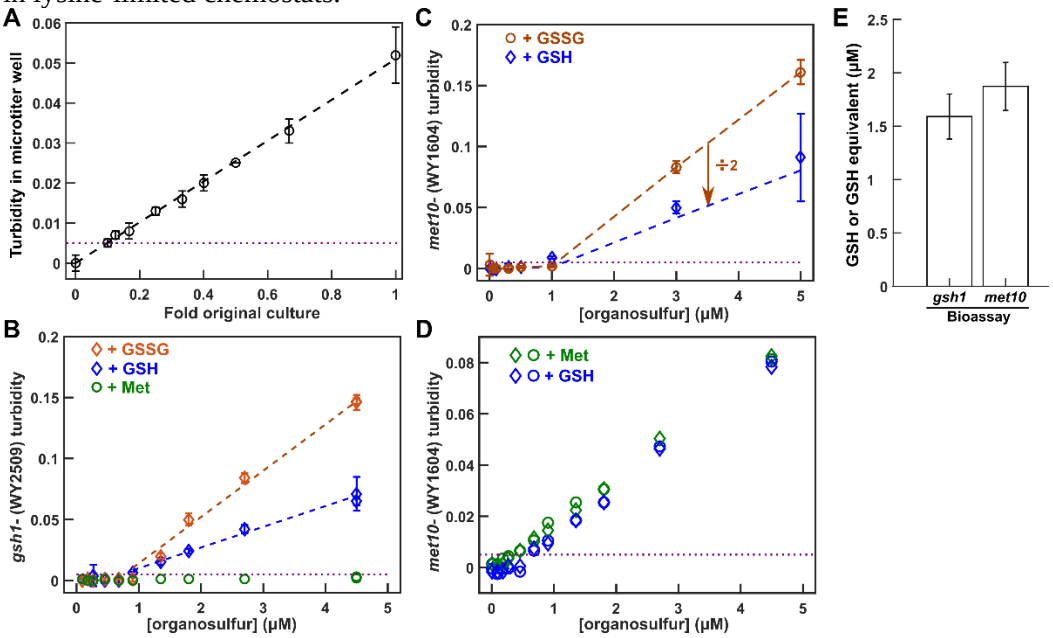

Fig S5. Lysine limitation increases GSH release rate

Fig S5 (**A, B**) Ancestral *lys2-* cells (WY1335) were cultured in excess lysine (turbidostats with doubling time of 1.5 hrs; magenta) or limited lysine (lysine-limited chemostats at doubling time of 8 hrs; green). Live and dead population densities were quantified using flow cytometry (Methods), and supernatant GSH concentrations were quantified using a fluorescence-based HPLC assay [50] (Methods). Different symbols represent independent experiments. The dotted line in **B** marks the sensitivity of the HPLC assay. (**C**) Higher GSH release rate during lysine limitation. GSH release rate by *lys2-* was calculated from the average steady-state GSH concentration, steady-state live cell density, and dilution rate (Methods). P-value was derived from a one-tailed t-test assuming equal variance. (**D**) GSH release rates were comparable between the ancestral *lys2-* (circles) and an evolved *lys2-* clone (crosses; WY2429 which contains an *ecm21* mutation and Chromosome 14 duplication and thus exhibit improved affinity for lysine). Here, cells were grown in lysine-limited chemostats (8-hr doubling). In (**C**) and (**D**), different colors correspond to experiments done on different days.

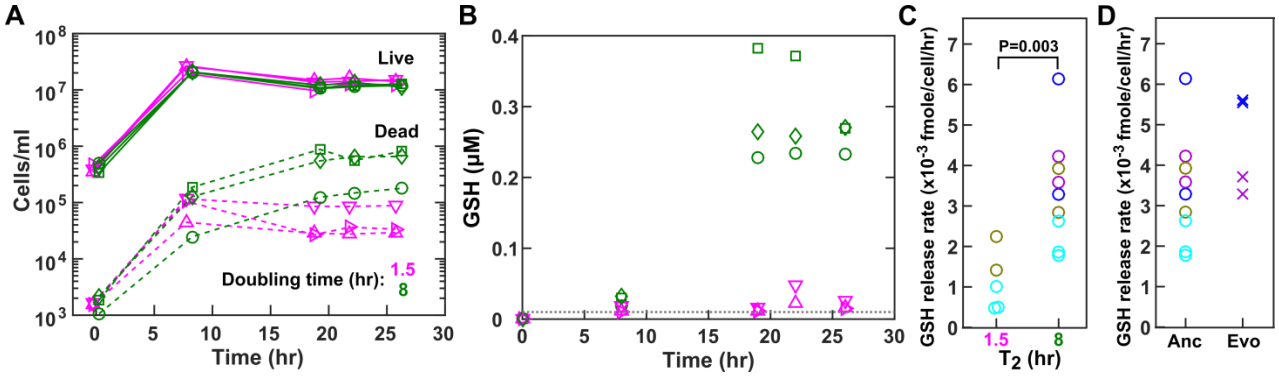

Fig S6. GSH is likely released by live ancestral and evolved *lys2-* cells.

Fig S6 Ancestral (WY1335, circles) and evolved (WY2429, crosses) *lys-* cells were cultured in lysine-limited chemostats (doubling time 8 hrs). Intracellular metabolites were extracted from cells to quantify fmole GSH/cell (brown). We quantified dead cell density and the concentrations of GSH in culture supernatants. We then calculated the theoretical amount that would need to be inside an average cell in order for cell lysis alone to explain the supernatant concentrations (purple). Since the theoretical amount was higher than the actual amount in all experiments, GSH is likely released by live cells. GSH was quantified using HPLC, and dead cell density was quantified using flow cytometry (Methods). Here, each column corresponds to an experiment. Day-to-day variations exist, but the trend is clear across days.

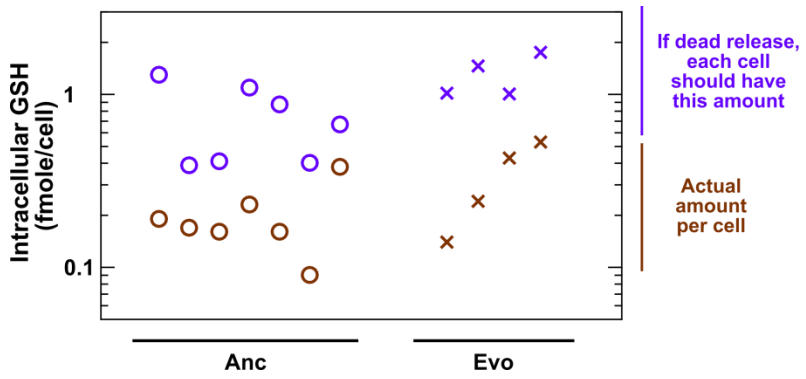

Fig S7. Negative frequency-dependent selection for *lys⁻orgS⁻*.

Fig S7 BFP-tagged *lys⁻orgS⁻* (WY2072 or WY2073) and mCherry-tagged *lys⁻* (WY2039 or WY2045) were competed in a lysine-limited environment by coculturing with a lysine-releasing strain (WY1340). Strain ratios over time were measured by flow cytometry (Figure 3). For each trajectory, we computed the slope of ln(*lys⁻orgS⁻*: *lys⁻*) over three consecutive time points, and chose the steepest slope. Since our time unit was generation, we divided this slope (/generation) by ln2/generation and obtain a dimensionless number representing the relative fitness difference between *lys⁻orgS⁻* and *lys⁻*. We then plotted the relative fitness difference against the fraction of *lys⁻orgS⁻* at the beginning of the time window used to calculate the steepest slope. Dotted line marks equal fitness between the two strains.

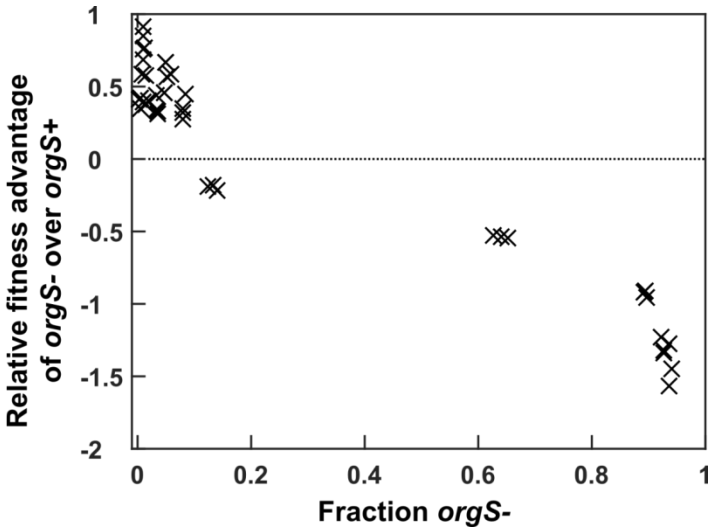

Fig S8. *lys⁻orgS⁻* survives lysine limitation better than *lys⁻* during sulfur limitation

Fig S8 *lys⁻* (WY2429, blue), *lys⁻orgS⁻* (WY1604, orange), and *lys⁻orgS⁻atg5⁻* (WY2370, green) lysine auxotrophs were grown in SD+ excess lysine (164 µM) and excess GSH (134 µM) to exponential phase. These cells were washed and starved in SD for 5 hours prior to imaging in indicated conditions with (crosses) or without (circles) 1 µM rapamycin in the absence of lysine. Total fluorescence normalized against time zero are plotted. (**A**) When GSH was limited, *lys⁻orgS⁻*survived better than *lys⁻* (orange circles above blue circles). TORC1 inhibition by rapamycin improved the survival of both *lys⁻orgS⁻* and *lys⁻* to comparable levels (orange and blue crosses). *lys⁻orgS⁻atg5⁻* survived poorly even when TORC1 was shut down (green crosses). (**B**) At high GSH, both *lys⁻orgS⁻* and *lys⁻* survived poorly (orange circles trending down at a similar slope as blue circles), and this poor viability was rescued by rapamycin (blue and orange crosses). *lys⁻orgS⁻atg5⁻* survived poorly in the presence or absence of rapamycin (green). Error bars represent two SEM (standard error of mean) from six wells.

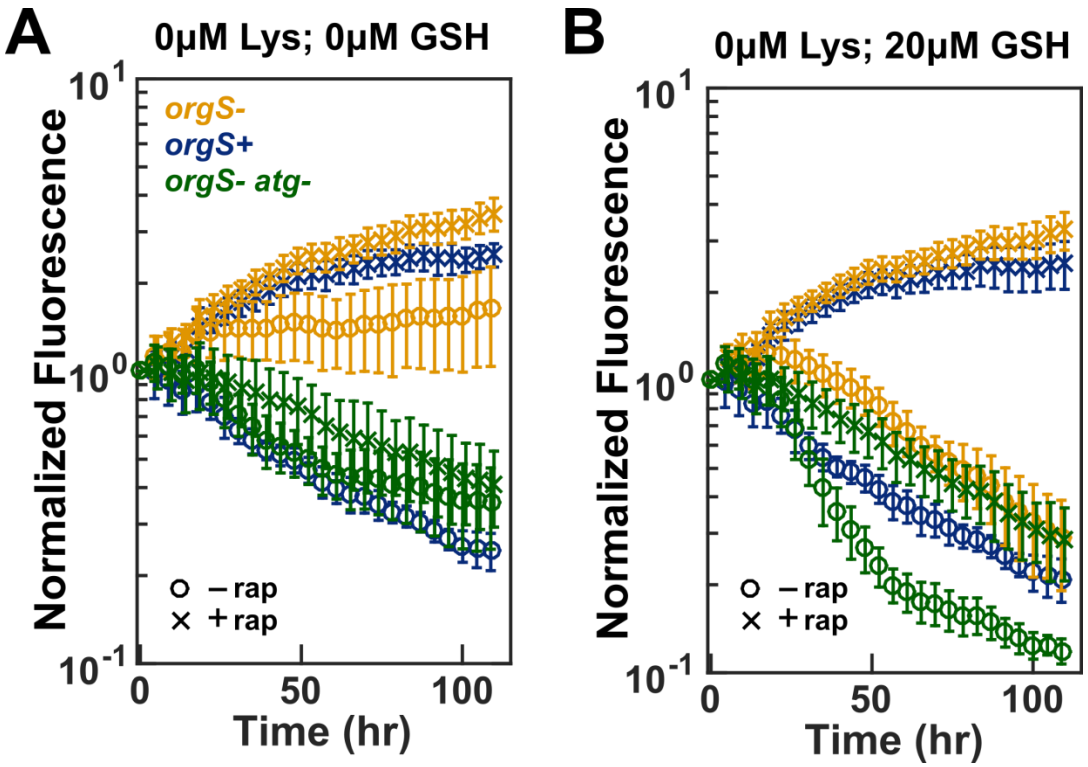

Fig S9. Comparing the growth and death profiles of *lys⁻orgs⁻* and *lys⁻* cells

Fig S9 *lys⁻* (WY2429, blue) and *lys⁻orgs⁻* (WY1604, orange) cells were grown in SD+ excess lysine (164 µM) and excess GSH (134 µM) to exponential phase. These cells were washed and starved in YNB+2% (w/v) glucose for 24 hours and imaged in various concentrations of GSH and lysine. During the growth phase, *lys⁻* grew faster than *lys⁻orgs⁻*. After lysine was exhausted, *lys⁻orgs⁻* survived better than *lys⁻*. Note that in the microscopy assay, the minimal medium did not contain GS-X or other excreted compounds found in culture supernatants. Regardless, and consistent with the competition experiment, *lys⁻orgs⁻* cells grew faster than *lys⁻* cells under certain conditions. In this experiment, at 2 µM GSH and 0.1 µM lysine, the maximal growth rate achieved by *lys⁻orgs⁻* was 0.153±0.009/hr (mean ± 2 standard error of mean), greater than the 0.133±0.004/hr achieved by *lys⁻*. Fluorescence intensities of various time points are normalized against that at time zero.

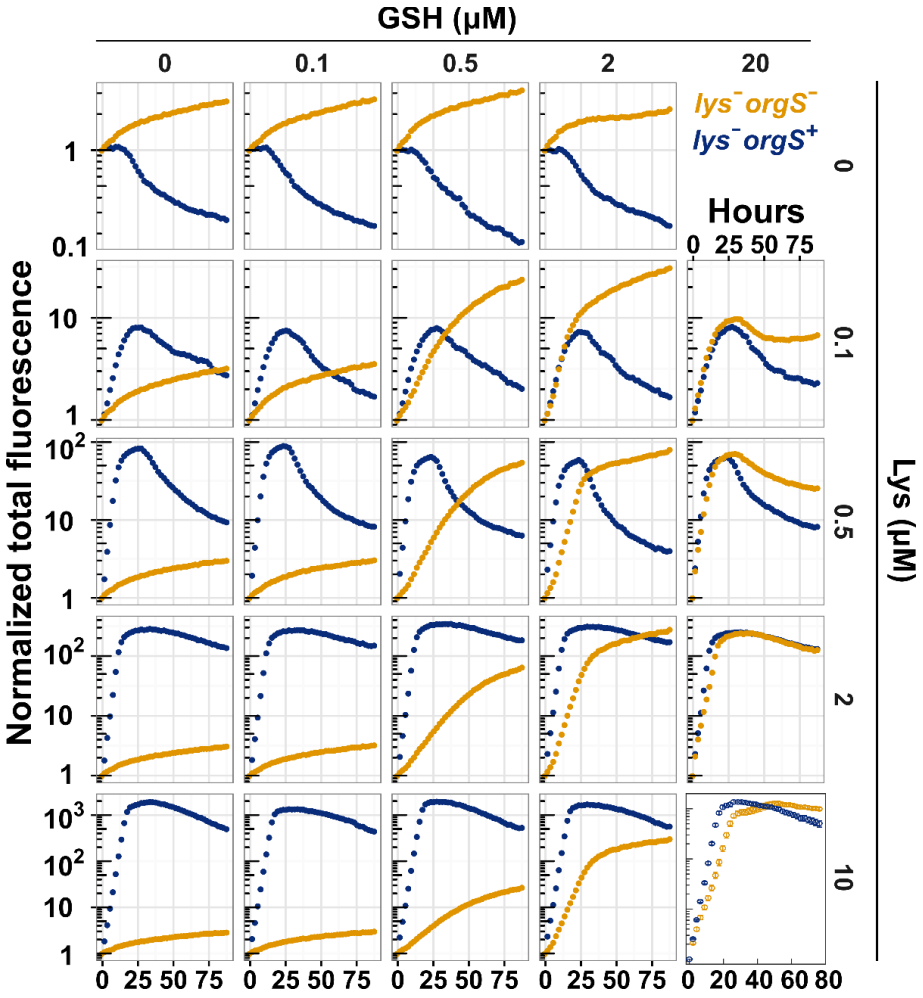

Fig S10. Continuous culturing device

The continuous culturing device (**A**) consists of six channels which can independently operate as a chemostat or turbidostat. Each channel (**B**) consists of a vessel containing the culture, a magnetic stirrer, an LED-phototransistor optical detector for OD measurement, a computer activated pump, a media reservoir, and a scale for measuring media reservoir (and flow rate). A LabView program running on the CPU uses data from the scale or optical detector to control the pump, and maintain a constant average OD in turbidostat mode, or a constant average flow rate in chemostat mode. Each vessel (**C**) consists of a Pyrex test tubes modified by adding a waste outlet of adequate diameter and slope to ensure a reliable flow of waste driven by gravity. The vessel's rubber stopper was outfitted with a sampling port consisting of a needle that can be raised and lowered through a seal provided by a segment of PharMed tubing. The tightness of the seal can be adjusted using a Zip-tie, allowing easy motion of the needle, while maintaining its position when stationary. Glass tubing? The six vessels, stirrers, and photodetectors are held in position in a frame cut from an aluminum bar. The signal from each phototransistor was converted to a voltage using an op-amp current to voltage converter (**B**). (**E**) Reactor volume averages 43 ml. Individual reactor volume was used for converting doubling time to flow rate, and was measured to ~0.5 ml resolution (limited by minimum outflow drop size; error bar).

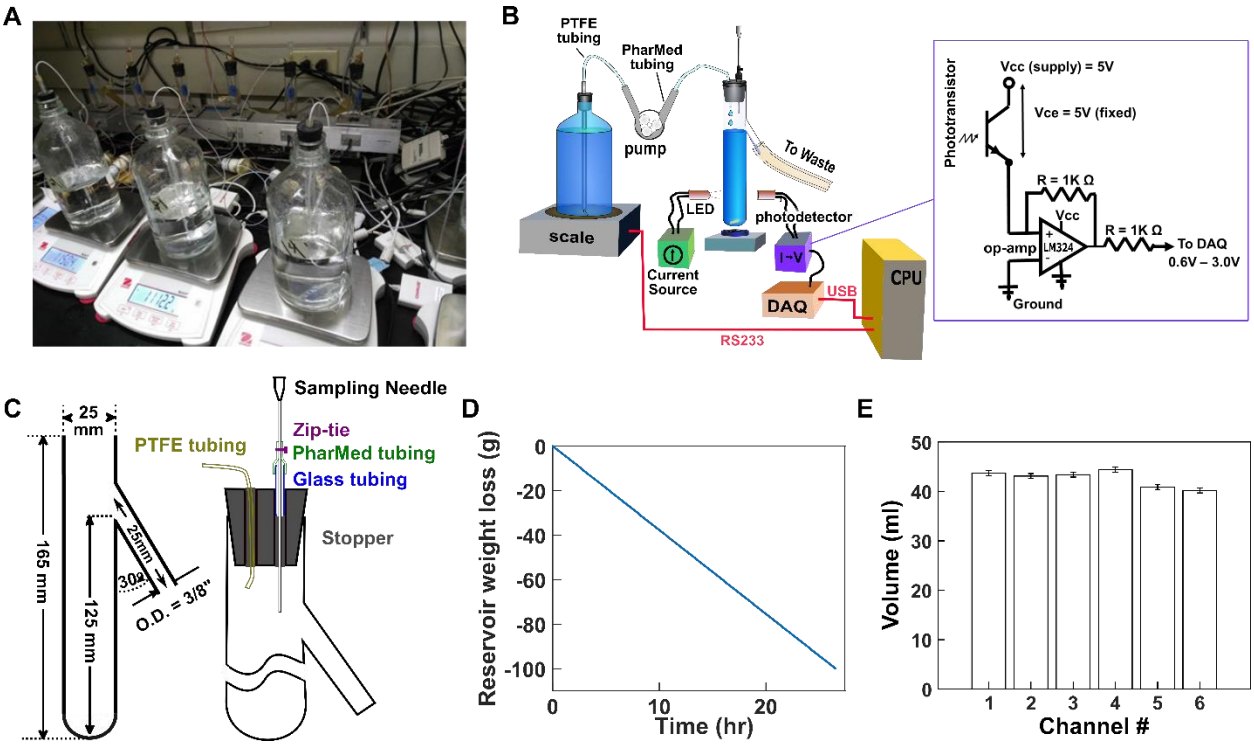

Table S1. Strains used in this study.

Table S2. Mutations in evolved clones

Table S2 All nine clones with the alias "ACI" are from chemostat evolution experiment. All other clones are from coculture evolution experiments, a fraction of which (i.e. "CT" strains) are from an earlier study [13]. For WY2467, earlier experiments noted that the strain failed to grow in SD + lysine. We identified it as *met*-, but its genetic basis is unclear since among identified mutations, none is known to affect methionine biosynthesis. Alternating blue and white shading is to facilitate visualization. Green shading: auxotroph. Orange shading: a prototrophic clone isolated from the same sample as the neighboring auxotrophic clone.

References

1. Slavov N, Botstein D. Coupling among growth rate response, metabolic cycle, and cell division cycle in yeast. Mol Biol Cell. 2011 Jun 15;22(12):1997–2009. PMID: 21525243

2. Huang J, Klionsky DJ. Autophagy and Human Disease. Cell Cycle. 2007 Aug 1;6(15):1837–1849. PMID: 17671424

3. Jewell JL, Guan K-L. Nutrient signaling to mTOR and cell growth. Trends Biochem Sci. 2013 May 1;38(5):233–242.

4. Laplante M, Sabatini DM. mTOR Signaling in Growth Control and Disease. Cell. 2012 Apr 13;149(2):274–293.

5. Davie E, Forte GMA, Petersen J. Nitrogen Regulates AMPK to Control TORC1 Signaling. Curr Biol. 2015 Feb 16;25(4):445–454. PMCID: PMC4331286

6. Sutter BM, Wu X, Laxman S, Tu BP. Methionine Inhibits Autophagy and Promotes Growth by Inducing the SAM-Responsive Methylation of PP2A. Cell. 2013 Jul 18;154(2):403–415. PMID: 23870128

7. Boer VM, Amini S, Botstein D. Influence of genotype and nutrition on survival and metabolism of starving yeast. Proc Natl Acad Sci. 2008 May 13;105(19):6930–6935.

8. Slavov N, Botstein D. Decoupling nutrient signaling from growth rate causes aerobic glycolysis and deregulation of cell size and gene expression. Mol Biol Cell. 2013 Jan 15;24(2):157–168. PMCID: PMC3541962

9. Pópulo H, Lopes JM, Soares P. The mTOR Signalling Pathway in Human Cancer. Int J Mol Sci. 2012 Feb 10;13(2):1886–1918. PMCID: PMC3291999

10. Waite AJ, Shou W. Adaptation to a new environment allows cooperators to purge cheaters stochastically. Proc Natl Acad Sci. 2012 Nov 20;109(47):19079–19086. PMID: 23091010

11. Lin CH, MacGurn JA, Chu T, Stefan CJ, Emr SD. Arrestin-Related Ubiquitin-Ligase Adaptors Regulate Endocytosis and Protein Turnover at the Cell Surface. Cell. 2008 Nov 14;135(4):714–725. PMID: 18976803

12. Hart, Samuel F.M., Pineda, Jose M.B., Chen, Chichun, Green, Robin, Shou, Wenying. Disentangling self-serving from win-win mutations in a mutualistic microbial community. Submitted.

13. Masselot M, Robichon-Szulmajster H. Methionine biosynthesis in Saccharomyces cerevisiae: I. Genetical analysis of auxotrophic mutants. MGG Mol Gen Genet [Internet]. 1975 [cited 2014 Feb 1];139(2). Available from: http://rd.springer.com/article/10.1007%2FBF00264692

14. Ishikawa T. The ATP-dependent glutathione S-conjugate export pump. Trends Biochem Sci. 1992;17(11):463–468.

15. Grant CM, MacIver FH, Dawes IW. Glutathione is an essential metabolite required for resistance to oxidative stress in the yeastSaccharomyces cerevisiae. Curr Genet. 1996 May 1;29(6):511–515.

16. Rebbeor JF, Connolly GC, Dumont ME, Ballatori N. ATP-dependent transport of reduced glutathione in yeast secretory vesicles. Biochem J. 1998 Sep 15;334 (Pt 3):723–729. PMCID: PMC1219743

17. Gresham D, Dunham MJ. The enduring utility of continuous culturing in experimental evolution. Genomics. 2014 Dec;104(6, Part A):399–405.

18. Zamenhof S, Eichhorn HH. Study of microbial evolution through loss of biosynthetic functions: establishment of “defective” mutants. Nature. 1967 Nov 4;216(5114):456–458. PMID: 4964402

19. D’Souza G, Waschina S, Pande S, Bohl K, Kaleta C, Kost C. Less Is More: Selective Advantages Can Explain the Prevalent Loss of Biosynthetic Genes in Bacteria. Evolution. 2014 Sep 1;68(9):2559–2570.

20. Laland KN, Odling-Smee FJ, Feldman MW. Evolutionary consequences of niche construction and their implications for ecology. Proc Natl Acad Sci. 1999 Aug 31;96(18):10242–10247. PMID: 10468593

21. Morris JJ, Lenski RE, Zinser ER. The Black Queen Hypothesis: evolution of dependencies through adaptive gene loss. mBio. 2012;3(2). PMID: 22448042

22. Stams AJM, Bok FAM de, Plugge CM, Eekert MHA van, Dolfing J, Schraa G. Exocellular electron transfer in anaerobic microbial communities. Environ Microbiol. 2006;8(3):371–382.

23. Hillesland Kristina Linnea. Evolution on the bright side of life: microorganisms and the evolution of mutualism. Ann N Y Acad Sci [Internet]. 2017 Nov 30 [cited 2018 Apr 11];0(0). Available from: https://nyaspubs.onlinelibrary.wiley.com/doi/full/10.1111/nyas.13515

24. Mee MT, Collins JJ, Church GM, Wang HH. Syntrophic exchange in synthetic microbial communities. Proc Natl Acad Sci. 2014 Apr 28;201405641. PMID: 24778240

25. Beliaev AS, Romine MF, Serres M, Bernstein HC, Linggi BE, Markillie LM, Isern NG, Chrisler WB, Kucek LA, Hill EA, Pinchuk GE, Bryant DA, Steven Wiley H, Fredrickson JK, Konopka A. Inference of interactions in cyanobacterial–heterotrophic co-cultures via transcriptome sequencing. ISME J. 2014 Nov;8(11):2243–2255.

26. Helliwell KE, Wheeler GL, Leptos KC, Goldstein RE, Smith AG. Insights into the Evolution of Vitamin B12 Auxotrophy from Sequenced Algal Genomes. Mol Biol Evol. 2011 Oct 1;28(10):2921–2933.

27. Carini P, Campbell EO, Morré J, Sañudo-Wilhelmy SA, Cameron Thrash J, Bennett SE, Temperton B, Begley T, Giovannoni SJ. Discovery of a SAR11 growth requirement for thiamin’s pyrimidine precursor and its distribution in the Sargasso Sea. ISME J. 2014 Aug;8(8):1727–1738.

28. Rodionova IA, Li X, Plymale AE, Motamedchaboki K, Konopka AE, Romine MF, Fredrickson JK, Osterman AL, Rodionov DA. Genomic distribution of B-vitamin auxotrophy and uptake transporters in environmental bacteria from the C hloroflexi phylum. Environ Microbiol Rep. 2015;7(2):204–210.

29. Zengler K, Zaramela LS. The social network of microorganisms — how auxotrophies shape complex communities. Nat Rev Microbiol. 2018 Mar 29;1.

30. Jiang X, Zerfaß C, Feng S, Eichmann R, Asally M, Schäfer P, Soyer OS. Impact of spatial organization on a novel auxotrophic interaction among soil microbes. ISME J. 2018 Mar 23;1.

31. Paczia N, Nilgen A, Lehmann T, Gätgens J, Wiechert W, Noack S. Extensive exometabolome analysis reveals extended overflow metabolism in various microorganisms. Microb Cell Factories. 2012;11:122.

32. Ponomarova O, Gabrielli N, Sévin DC, Mülleder M, Zirngibl K, Bulyha K, Andrejev S, Kafkia E, Typas A, Sauer U. Yeast Creates a Niche for Symbiotic Lactic Acid Bacteria through Nitrogen Overflow. Cell Syst. 2017;5(4):345–357.

33. Kinnersley MA, Holben WE, Rosenzweig F. E Unibus Plurum: genomic analysis of an experimentally evolved polymorphism in Escherichia coli. PLoS Genet. 2009 Nov;5(11):e1000713. PMID: 19893610

34. Basan M, Hui S, Okano H, Zhang Z, Shen Y, Williamson JR, Hwa T. Overflow metabolism in Escherichia coli results from efficient proteome allocation. Nature. 2015 Dec 3;528(7580):99–104.

35. Szenk M, Dill KA, de Graff AMR. Why Do Fast-Growing Bacteria Enter Overflow Metabolism? Testing the Membrane Real Estate Hypothesis. Cell Syst. 2017 Aug 23;5(2):95–104.

36. Sies H. Glutathione and its role in cellular functions. Free Radic Biol Med. 1999 Nov 1;27(9):916–921.

37. Glutathione, Altruistic Metabolite in Fungi. 2004 Jan 1;49:1–76.

38. Dhaoui M, Auchère F, Blaiseau P-L, Lesuisse E, Landoulsi A, Camadro J-M, Haguenauer-Tsapis R, Belgareh-Touzé N. Gex1 is a yeast glutathione exchanger that interferes with pH and redox homeostasis. Mol Biol Cell. 2011 Jun 15;22(12):2054–2067. PMCID: PMC3113770

39. Elbaz-Alon Y, Morgan B, Clancy A, Amoako TNE, Zalckvar E, Dick TP, Schwappach B, Schuldiner M. The yeast oligopeptide transporter Opt2 is localized to peroxisomes and affects glutathione redox homeostasis. FEMS Yeast Res. 2014 Nov 1;14(7):1055–1067.

40. Petti AA, Crutchfield CA, Rabinowitz JD, Botstein D. Survival of starving yeast is correlated with oxidative stress response and nonrespiratory mitochondrial function. Proc Natl Acad Sci U S A. 2011 Nov 8;108(45):E1089-1098. PMCID: PMC3215077

41. Hu J, Fan L, Chen Q, Dong Y. RNA-Seq-based transcriptomic and metabolomic analysis reveal stress responses and programmed cell death induced by acetic acid in *Saccharomyces cerevisiae*. Sci Rep. 2017 Feb 17;7:42659.

42. Campbell K, Vowinckel J, Muelleder M, Malmsheimer S, Lawrence N, Calvani E, Miller-Fleming L, Alam MT, Christen S, Keller MA, Ralser M. Self-establishing communities enable cooperative metabolite exchange in a eukaryote. eLife. 2015 Oct 26;e09943.

43. Dykhuizen D. Selection for Tryptophan Auxotrophs of Escherichia coli in Glucose-Limited Chemostats as a Test of the Energy Conservation Hypothesis of Evolution. Evolution. 1978 Mar 1;32(1):125–150.

44. D'Souza G, Kost C. Experimental Evolution of Metabolic Dependency in Bacteria. PLOS Genet. 2016 Nov 4;12(11):e1006364.

45. Guthrie C, Fink GR. Guide to yeast genetics and molecular biology. Academic Press; 1991.

46. Hart SFM, Skelding D, Waite AJ, Burton J, Li X, Shou W. High-throughput quantification of microbial birth and death dynamics using fluorescence microscopy. Quant Biol. BIORXIV/2018/324269.

47. Skelding D, Hart SF, Vidyasagar T, Pozhitkov AE, Shou W. Developing a low-cost milliliter-scale chemostat array for precise control of cellular growth. Quant Biol. 2018;6(2):129–141.

48. Hart SFM, Mi H, Green R, Pineda JMB, Momeni B, Shou W. Resolving challenges in quantitative modeling of microbial community dynamics. PLoS Biol Accept.

49. Rosebrock AP, Caudy AA. Metabolite Extraction from Saccharomyces cerevisiae for Liquid Chromatography–Mass Spectrometry. Cold Spring Harb Protoc. 2017 Sep 1;2017(9):pdb.prot089086. PMID: 28864564

50. Yi L, Li H, Sun L, Liu L, Zhang C, Xi Z. A Highly Sensitive Fluorescence Probe for Fast Thiol-Quantification Assay of Glutathione Reductase. Angew Chem Int Ed. 2009 May 18;48(22):4034–4037.

51. Melamud E, Vastag L, Rabinowitz JD. Metabolomic Analysis and Visualization Engine for LC−MS Data. Anal Chem. 2010 Dec 1;82(23):9818–9826.

52. Hess DC, Lu W, Rabinowitz JD, Botstein D. Ammonium Toxicity and Potassium Limitation in Yeast. PLoS Biol. 2006 Oct 17;4(11):e351.

53. Novick A, Szilard L. Experiments on spontaneous and chemically induced mutations of bacteria growing in the Chemostat. Cold Spring Harb Symp Quant Biol. 1951 Jan;16:337–43.

54. Shou W, Ram S, Vilar JM. Synthetic cooperation in engineered yeast populations. Proc Natl Acad Sci USA. 2007;104:1877–1882. PMCID: 1794266

55. Thomas D, Surdin-Kerjan Y. Metabolism of sulfur amino acids in Saccharomyces cerevisiae. Microbiol Mol Biol Rev. 1997 Dec;61(4):503–532. PMCID: PMC232622